iScience

CellPress
OPEN ACCESS

Article

Radiomics and dosiomics for predicting radiation-induced hypothyroidism and guiding intensity-modulated radiotherapy

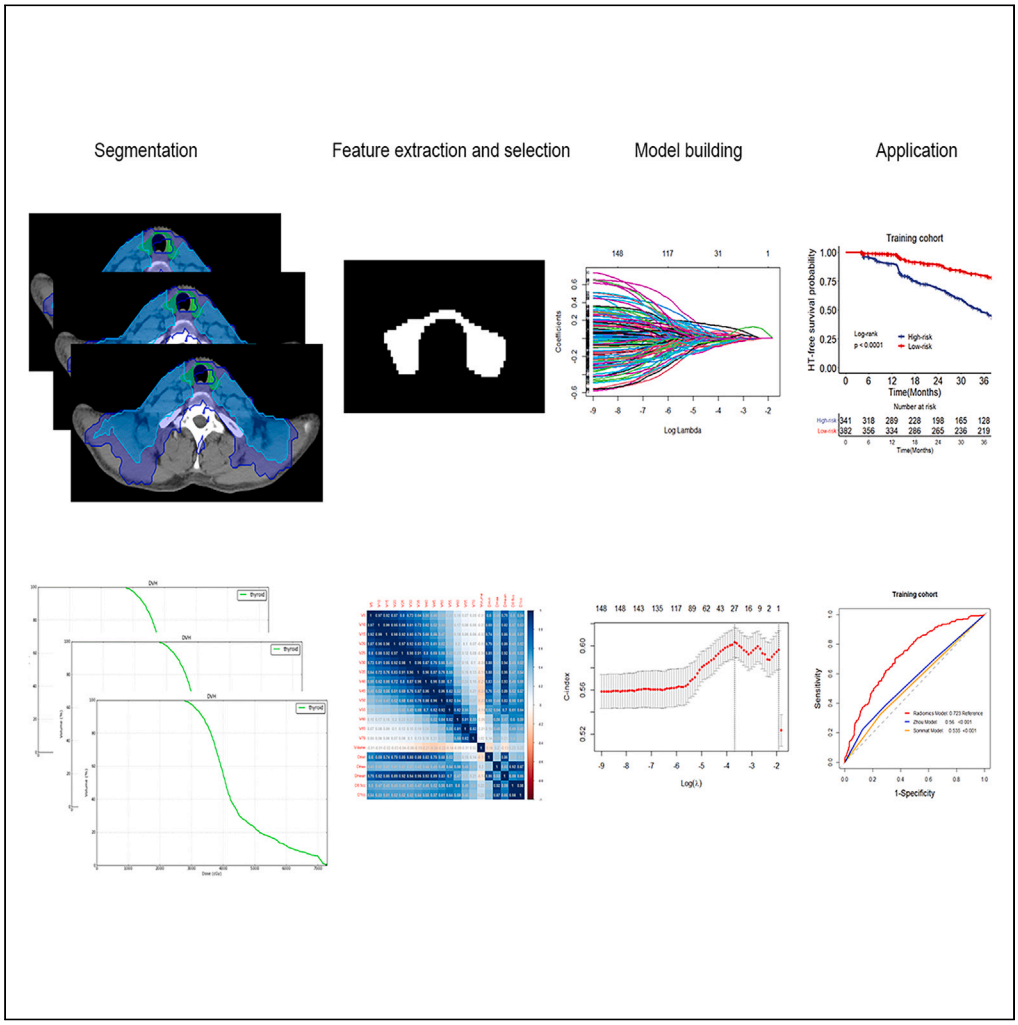

Shan-Shan Yang, Qing-He Peng, Ai-Qian Wu, ..., Fang-Yun Xie, Pu-Yun OuYang, Chun-Yan Chen

15626047198@163.com (A.-Q.W.)
xiefy@sysucc.org.cn (F.-Y.X.)
ouyangpy@sysucc.org.cn (P.-Y.O.)
chenchuny@sysucc.org.cn (C.-Y.C.)

Highlights

The multiview radiomics risk model can predict radiation-induced hypothyroidism

The multiview radiomics risk model performed better than the NTCP model

The multiview radiomics risk model can guide intensity-modulated radiotherapy

Yang et al., iScience *26*, 108394
December 15, 2023
https://doi.org/10.1016/j.isci.2023.108394

iScience

CellPress
OPEN ACCESS

Article

Radiomics and dosiomics for predicting radiation-induced hypothyroidism and guiding intensity-modulated radiotherapy

Shan-Shan Yang,[1,2,4] Qing-He Peng,[1,4] Ai-Qian Wu,[3,4,*] Bao-Yu Zhang,[1] Zhi-Qiao Liu,[1] En-Ni Chen,[1] Fang-Yun Xie,[1,*] Pu-Yun OuYang,[1,*] and Chun-Yan Chen[1,5,*]

SUMMARY

To guide individualized intensity-modulated radiotherapy (IMRT), we developed and prospectively validated a multiview radiomics risk model for predicting radiation-induced hypothyroidism in patients with nasopharyngeal carcinoma. And simulated radiotherapy plans with same dose-volume-histogram (DVH) but different dose distributions were redesigned to explore the clinical application of the multiview radiomics risk model. The radiomics and dosiomics were built based on selected radiomics and dosiomics features from planning computed tomography and dose distribution, respectively. The multiview radiomics risk model that integrated radiomics, dosiomics, DVH parameters, and clinical factors had better performance than traditional normal tissue complication probability models. And multiview radiomics risk model could identify differences of patient hypothyroidism-free survival that cannot be stratified by traditional models. Besides, two redesigned simulated plans further verified the clinical application and advantage of the multiview radiomics risk model. The multiview radiomics risk model was a promising method to predict radiation-induced hypothyroidism and guide individualized IMRT.

INTRODUCTION

Radiotherapy is the cornerstone of nasopharyngeal carcinoma treatment.[1] As intensity-modulated radiotherapy (IMRT) preserves organs at risk, patients' quality of life improves.[2] However, radiation-induced hypothyroidism has a higher incidence after IMRT than after 3-dimensional conformal radiotherapy.[3] The prevalence of primary hypothyroidism in nasopharyngeal carcinoma patients after IMRT ranges from 20% to 60%.[4,5] Hypothyroidism generally occurs within 5 years after radiotherapy, with a peak at 1–2 years.[3,6,7] If ignored, hypothyroidism may have an important impact on quality of life.

Dosimetric predictors for hypothyroidism included V_{40} (percentage of thyroid volume receiving more than 40 Gy), V_{45}, V_{50}, and thyroid volume.[8,9] Clinical factors such as age, N stage, and treatment, has also been proven as risk factors.[7,8] Thus, Zhou et al. developed a combined model of total tumor volume and N stage to predict the incidence of hypothyroidism.[7] Normal tissue complication probability (NTCP) models are commonly used for predicting radiation-induced complications.[10] However, notably, the aforementioned studies were based on only one-dimensional dosimetric factors or two-dimensional dose-volume histogram (DVH) curves. The same dosimetric parameters can be obtained from completely different dose distributions. Due to the lack of an effective model for evaluating the spatial information of the 3-dimensional dose distribution, it is difficult to choose an optimal treatment plan based on only dosimetric parameters. Whether different 3-dimensional dose distributions with same DVH parameters leads to different incidences of radiation-induced hypothyroidism remains to be verified. In addition, pretreatment planning computed tomography (CT) may also contain microscopic genetic heterogeneities of organs at risk and could predict the probability of hypothyroidism.

Radiomics can convert medical images to high-dimensional mineable data by high-throughput extraction of quantitative features,[11] which provides a method for mining the spatial information of medical images. While CT has been widely applied to improve predictive models by radiomics,[12] dosiomics can also be used for describing spatial features of 3-dimensional dose distribution to predict radiation-induced complications.[13,14] A study confirmed the outstanding performance of a dosiomics-based model in predicting radiation-induced complications in prostate cancer, and a model combining dosiomics and radiomics was also reported to significantly improve the performance of predicting

[1]Department of Radiation Oncology, Sun Yat-sen University Cancer Center, State Key Laboratory of Oncology in South China, Collaborative Innovation Center for Cancer Medicine, Guangdong Key Laboratory of Nasopharyngeal Carcinoma Diagnosis and Therapy, Guangdong Provincial Clinical Research Center for Cancer, Guangzhou, Guangdong 510060, China
[2]Department of Radiation Oncology, Shandong Provincial Hospital Affiliated to Shandong First Medical University, Jinan, Shandong 250021, China
[3]Department of Radiation Oncology, The First Affiliated Hospital of Guangzhou University of Chinese Medicine, Guangzhou, Guangdong 510405, China
[4]These authors contributed equally
[5]Lead contact
*Correspondence: 15626047198@163.com (A.-Q.W.), xiefy@sysucc.org.cn (F.-Y.X.), ouyangpy@sysucc.org.cn (P.-Y.O.), chenchuny@sysucc.org.cn (C.-Y.C.)
https://doi.org/10.1016/j.isci.2023.108394

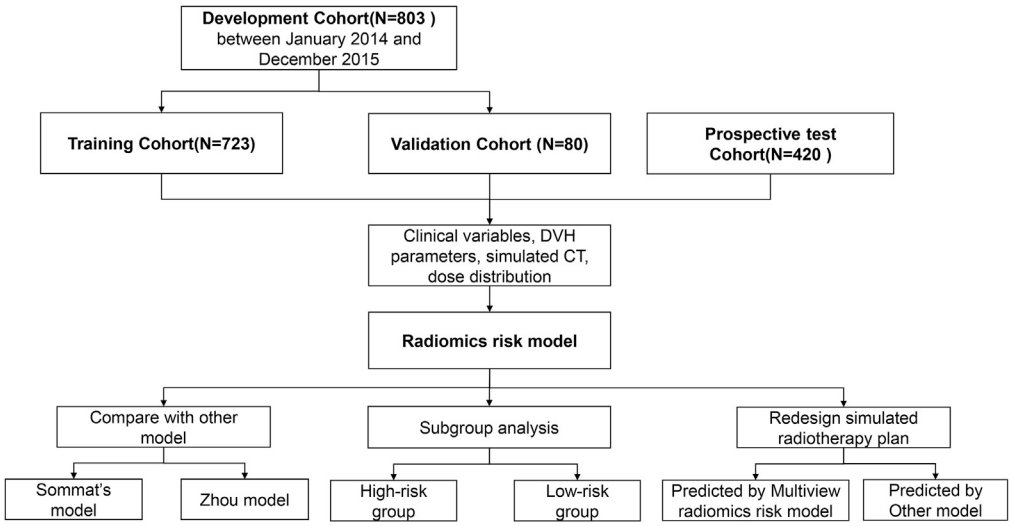

Figure 1. The workflow of this study
Abbreviation: CT, computed tomography; DVH, dose-volume histogram.

local control and acute weight loss.[15,16] Therefore, we aimed to develop and validate a multiview model that combines radiomics, dosiomics, DVH parameters, and clinical characteristics to predict radiation-induced hypothyroidism in nasopharyngeal carcinoma, and thus guide individualized IMRT.

RESULTS

Patient characteristics

There were 723, 80, and 420 patients in the training cohort, validation cohort, and prospective test cohort, respectively (Figure 1). With a median follow-up of 34, 37, and 22 months, 375 (53.34%), 48 (60.00%), and 191 (45.48%) patients were diagnosed with primary hypothyroidism in the training, validation, and prospective test cohorts, respectively. The baseline characteristics are shown in Table 1. Obviously, primary hypothyroidism tended to occur in younger and advanced N stage patients in the training and validation cohorts. With regard to the T stage and overall stage, there was no difference between euthyroid and hypothyroidism patients. The 3-year hypothyroidism-free survival rates were 63.9%, 64.0%, and 44.5%, respectively.

Development and prospective test of multiview radiomics risk model

After univariate Cox regression analysis, age and N stage were identified as potential predictors for hypothyroidism (Table S1). The Pearson correlation between twenty DVH parameters is shown in Figure S1. Since dosimetric parameters were highly correlated with each other, only V_{45} with a cutoff of 57% was selected for model building.

According to the selection process (Table S2), 20 dosiomics features and 27 radiomics features with nonzero coefficients in the LASSO-Cox model were retained for signature building in the training cohort (Figure S2). Imaging and segmentation perturbations were performed for robustness evaluation of the selected features. For the segmentation perturbations, the median intraclass correlation coefficients (ICCs) of features for test-retest and inter-rater analyses were 0.962 (interquartile ranges [IQR]: 0.796–0.975) and 0.912 (IQR: 0.813–0.974), respectively, while the median ICCs of features for modifying the field of view (FOV) and reconstruction mode were 0.813 (IQR: 0.792–0.922) and 0.876 (IQR: 0.797–0.962) in the imaging perturbations, respectively. And the median ICCs of dosiomics features for modifying the dose calculation grid size were 0.869 (IQR: 0.850–0.975), which indicated robustness of the selected features. Based on the selected features and corresponding coefficients presented in Table S3, radiomics signature and dosiomics signature were calculated. The C-indices of radiomics signature and dosiomics signature were 0.671 (95% confidence interval [CI]: 0.630–0.712) and 0.652 (95% CI: 0.611–0.694), respectively, in the prospective test cohort (Table S4).

When multivariable Cox regression analysis was conducted, the variables including radiomics signature, dosiomics signature, V_{45}, age, and N stage were the independent predictive factors for hypothyroidism-free survival (Table S5). Consequently, a multiview radiomics risk model and corresponding nomogram were established to predict individualized hypothyroidism (Figure 2). The calibration curves displayed favorable agreement between the predicted probability and the actual outcome in each cohort (Figure 2). As shown in Table 2, the C-indices of multiview radiomics risk model were 0.681 (95% CI: 0.653–0.710), 0.704 (95% CI: 0.632–0.777), and 0.725 (95% CI: 0.687–0.762) in the training, validation, and prospective test cohorts, respectively, and the three-year time-dependent AUC of the multiview radiomics risk model was 0.723 (95% CI: 0.681–0.765), 0.777 (95% CI: 0.663–0.892), and 0.763 (95% CI: 0.699–0.827) in the corresponding cohort. The cutoff value of the radiomics nomogram point was determined to be 94 by time-dependent receiver operating characteristic (ROC). Thus, 341, 41, and

Table 1. The clinical characteristics of patients with non-HT and HT in the training, validation, and prospective test cohorts

	Training cohort			Validation cohort			Prospective test cohort		
	Non-HT	HT		Non-HT	HT		Non-HT	HT	
	N = 348	N = 375	p	N = 32	N = 48	p	N = 229	N = 191	p
Sex			0.067			1			0.003
Female	95 (27.3)	127 (33.9)		11 (34.4)	16 (33.3)		56 (24.5)	73 (38.2)	
Male	253 (72.7)	248 (66.1)		21 (65.6)	32 (66.7)		173 (75.5)	118 (61.8)	
Age			<0.001			0.819			0.001
<45	155 (44.5)	236 (62.9)		15 (46.9)	25 (52.1)		94 (41.0)	110 (57.6)	
≥45	193 (55.5)	139 (37.1)		17 (53.1)	23 (47.9)		135 (59.0)	81 (42.4)	
T stage			0.782			0.930			0.748
T1	30 (8.6)	32 (8.5)		4 (12.5)	5 (10.4)		13 (5.7)	12 (6.3)	
T2	53 (15.2)	65 (17.3)		4 (12.5)	7 (14.6)		23 (10.0)	19 (9.9)	
T3	181 (52.0)	182 (48.5)		17 (53.1)	23 (47.9)		131 (57.2)	117 (61.3)	
T4	84 (24.1)	96 (25.6)		7 (21.9)	13 (27.1)		62 (27.1)	43 (22.5)	
N stage			0.064			0.016			0.108
N0	55 (15.8)	37 (9.9)		6 (18.8)	4 (8.3)		28 (12.2)	11 (5.8)	
N1	127 (36.5)	142 (37.9)		19 (59.4)	17 (35.4)		89 (38.9)	80 (41.9)	
N2	123 (35.3)	134 (35.7)		3 (9.4)	18 (37.5)		68 (29.7)	67 (35.1)	
N3	43 (12.4)	62 (16.5)		4 (12.5)	9 (18.8)		44 (19.2)	33 (17.3)	
Overall stage			0.635			0.112			0.611
I	13 (3.7)	15 (4.0)		3 (9.4)	0 (0.0)		4 (1.7)	4 (2.1)	
II	38 (10.9)	41 (10.9)		3 (9.4)	2 (4.2)		19 (8.3)	14 (7.3)	
III	181 (52.0)	178 (47.5)		15 (46.9)	24 (50.0)		108 (47.2)	102 (53.4)	
IV	116 (33.3)	141 (37.6)		11 (34.4)	22 (45.8)		98 (42.8)	71 (37.2)	
Treatment			0.026			0.476			0.301
RT alone	38 (10.9)	27 (7.2)		3 (9.4)	1 (2.1)		20 (8.7)	9 (4.7)	
CCRT	163 (46.8)	151 (40.3)		13 (40.6)	24 (50.0)		107 (46.7)	87 (45.5)	
IC + CCRT	139 (39.9)	190 (50.7)		15 (46.9)	22 (45.8)		98 (42.8)	89 (46.6)	
IC + RT	8 (2.3)	7 (1.9)		1 (3.1)	1 (2.1)		4 (1.7)	6 (3.1)	

Abbreviation: CCRT, concurrent chemoradiotherapy; HT, hypothyroidism; IC, induction chemotherapy; RT, radiotherapy.

215 patients with ≥94 nomogram points were divided into high-risk group in the training, validation, and prospective test cohorts, while 382, 39, and 205 patients with <94 nomogram points were classified into the low-risk group. Patients in the low-risk group had better hypothyroidism-free survival rates than patients in the high-risk group in all cohorts (all $p < 0.001$, Figure S3).

Advantages of the multiview radiomics risk model

For comparison, the performance of Sommat's model of V_{40} [7] and Zhou's model of thyroid volume plus N stage [6] were also evaluated. The C-indices of Sommat's model were 0.514, 0.538, and 0.536 in the training, validation, and prospective test cohorts, respectively, and Zhou's model had C-indices of 0.549, 0.571, and 0.629. The multiview radiomics risk model had higher C-indices than Sommat's model and Zhou's model (all $p < 0.001$, Table 2). Similarly, Figure S4 also shows the AUCs of multiview radiomics risk model were higher than those of Sommat's model and Zhou's model in all cohorts (Table 2, all $p \leq 0.002$). In addition, the decision curve analysis showed that multiview radiomics risk model had higher net benefits than Sommat's model and Zhou's model, when the threshold probability ranged from 0.030 to 0.664 (Figure S5).

In the prospective test cohort, 357 and 63 patients were divided into low-risk and high-risk groups by Sommat's model of V_{40}, while 352 and 68 patients were classified into low-risk and high-risk groups, respectively, by Zhou's model of thyroid volume plus N stage (Table S6). Notably, among the two undistinguished low-risk groups stratified by Sommat's model and Zhou's model, the multiview radiomics risk model could still distinguish 3-year hypothyroidism-free survival (70.4% vs. 26.2% in the $V_{40} < 85\%$ set; 68.5% vs. 26.1% in the low-risk group by Zhou's model; all $p < 0.001$, Figures 3A and 3B). In contrast, in the high- or low-risk groups stratified by multiview radiomics model, both Sommat's model and Zhou's model were unable to distinguish hypothyroidism-free survival (all $p > 0.05$, Figures 3C–3F)

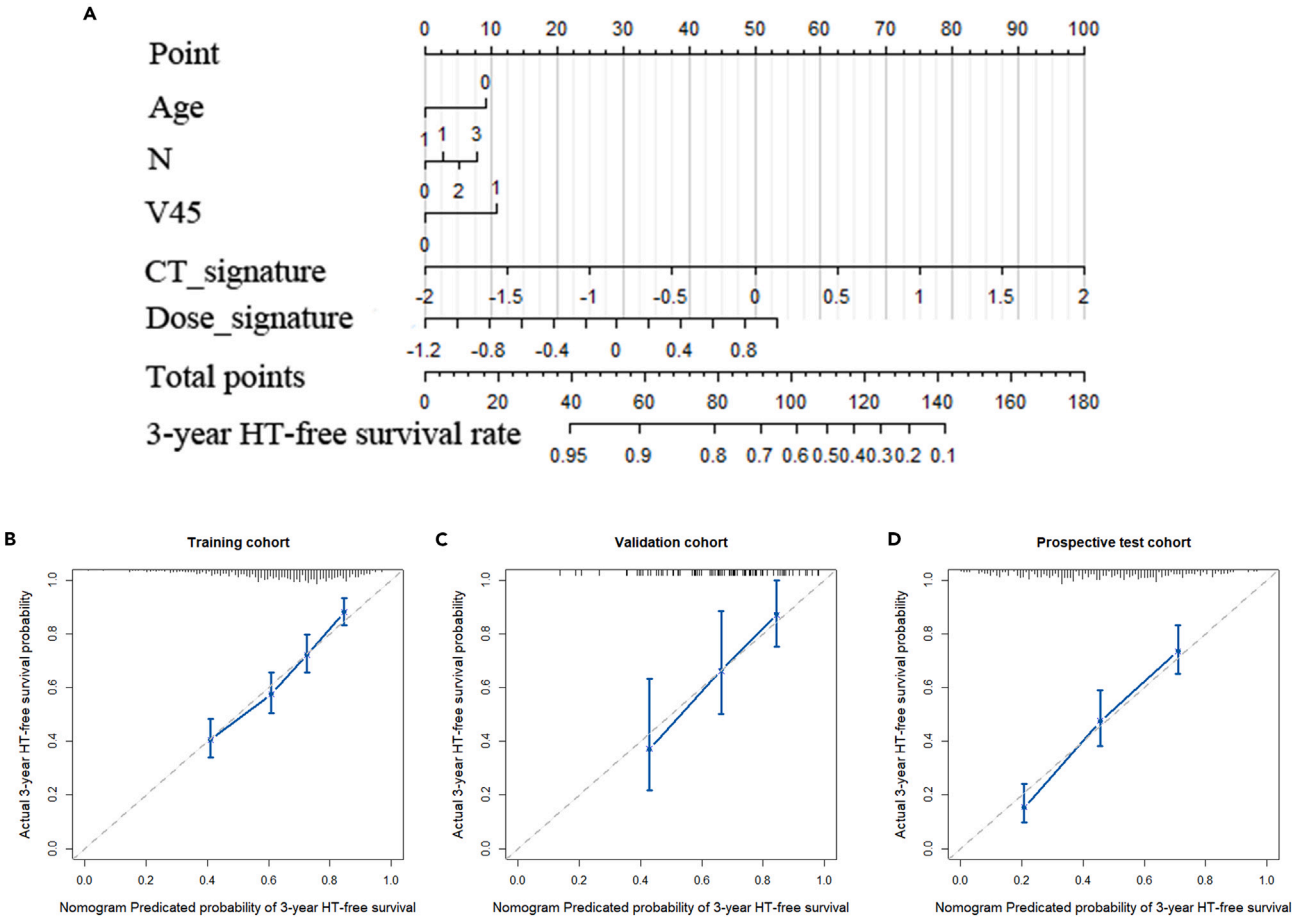

Figure 2. Nomogram and calibration curves of multiview radiomics risk model

Radiomics risk nomogram (A) and calibration curves in the training (B), validation (C), and prospective test cohort (D).

Abbreviation: CT, computed tomography; HT, hypothyroidism.

Clinical application of the multiview radiomics risk model

The characteristics of 50 randomly selected test patients are listed in Table S7. With the same dose prescription and constraints, three simulated treatment plans of each patient had target coverage higher than 95%. Simulated plan 1 had the same V_{45} to the thyroid but a different dose distribution than simulated plan 2, while simulated plan 3 was nearly the same as the irradiation treatment plan (all $p \geq 0.5$, Figure 4). There was a significant difference in the median 3-year hypothyroidism-free survival probability predicted by the multiview radiomics risk model between simulated plan 1 and plan 2 (69.00% vs. 72.86%, $p < 0.001$). Additionally, the median 3-year predicted hypothyroidism-free survival probability of simulated plan 3 (68.23%) was different from those of simulated plan 1 and plan 2 (all $p \leq 0.005$). However, the predicted hypothyroidism-free survival probability of simulated plan 1 by Sommat's model (67.14%) or Zhou's model (65.84%) was the same as that of simulated plan 2.

DISCUSSION

In this large cohort study, we developed and prospectively validated a multiview radiomics risk model to predict hypothyroidism-free survival rates and guide individualized IMRT. The multiview model combining radiomics, dosiomics, DVH parameters, and clinical factors performed better than the existing model. The redesigned simulated plans with different dose distributions had significant differences in hypothyroidism-free survival rates predicted by the multiview radiomics risk model, which further verified its clinical application.

In accordance with a previous study,[17] primary hypothyroidism had a high incidence of approximately 50% after IMRT in this study, indicating the importance of identifying predictors and regularly screening thyroid function. However, thyroid function monitoring is not routine after radiotherapy in clinical practice. Thus, building an effective multiview model for predicting radiation-induced hypothyroidism is urgently needed. Younger patients tended to suffer radiation-induced hypothyroidism more than older patients in our study. Similarly, several studies also reported that younger patients had a higher incidence of primary hypothyroidism.[8,17] Certainly, as shown in our study, the advanced

Table 2. Concordance indices and 3-year AUCs of different models in the training, internal test, prospective test, and external test cohorts

	Training cohort				Validation cohort				Prospective test cohort			
	C-index (95% CI)	P	3-year AUC (95% CI)	p	C-index (95% CI)	p	3-year AUC (95% CI)	p	C-index (95% CI)	p	3-year AUC (95% CI)	p
Sommat's model	0.514 (0.490–0.537)	<0.001	0.535 (0.496–0.574)	<0.001	0.538 (0.461–0.615)	<0.001	0.556 (0.435–0.677)	<0.001	0.536 (0.510–0.562)	<0.001	0.583 (0.540–0.626)	<0.001
Zhou's model	0.549 (0.518–0.581)	<0.001	0.560 (0.513–0.607)	<0.001	0.571 (0.491–0.652)	<0.001	0.591 (0.457–0.725)	0.001	0.629 (0.589–0.669)	<0.001	0.675 (0.609–0.741)	0.002
Radiomics risk model	0.681 (0.653–0.710)	RE	0.723 (0.681–0.765)	RE	0.704 (0.632–0.777)	RE	0.777 (0.663–0.892)	RE	0.725 (0.687–0.762)	RE	0.763 (0.699–0.827)	RE

Abbreviation: AUC, area under the curve; C-indices, concordance index; CI, confidence interval; RE, reference.

N stage was significantly related to hypothyroidism since the thyroid was more likely to be irradiated in patients with cervical lymph node metastasis.[7] In addition, studies have shown that the early T stage is an independent factor for predicting hypothyroidism,[8,18] as they assumed that a high dose to the pituitary in patients with advanced T stage might prevent the thyroid-stimulating hormone (TSH) from increasing. However, the postulation cannot be validated in our study. Since the whole pituitary was reoutlined, it was almost impossible to identify the adenohypophysis in which TSH was produced accurately. Considering the sharp drop in dose to organs at risk in IMRT era, dosimetric parameters to the whole pituitary cannot represent the dose to adenohypophysis. Therefore, patients with central hypothyroidism were excluded from this study. Although the median follow-up time of 22 months in the prospective test cohort was slightly short, we can still draw reliable conclusions since the peak incidence of hypothyroidism was 1–2 years after radiotherapy.

There was no doubt that DVH parameters played a critical role in predicting hypothyroidism, and the NTCP model has been commonly used in clinical practice. Previous studies have reported that various parameters including V_{30}, V_{35}, V_{40}, V_{50} and thyroid volume, are strongly related to hypothyroidism.[7,8,19] However, the optimal DVH parameter has not yet been determined, and the dose constraint to the thyroid has also not been reported in Quantitative Analyses of Normal Tissue Effects in the Clinic (QUANTEC). Given the strong correlation between DVH parameters, V_{45} with maximum time-dependent AUC was selected in this study.

With the rapid advancement of radiotherapy, the current one-dimensional and two-dimensional methods of evaluating treatment planning can no longer meet the complex dose distributions. Therefore, this study used the radiomics method to extract spatial features from planning CT and three-dimensional dose distribution. Image segmentation is the most critical and basic step for radiomics since the features are extracted from the segmentation region. In this study, all thyroids were reoutlined by a radiation oncologist with ten years of experience and checked by an expert radiation oncologist. Feature selection was the most challenging step for our study. To avoid overfitting and reduce irrelevant features, LASSO-Cox, which can effectively solve the multicollinearity problem of high-dimensional data, was applied to determine important features for predicting hypothyroidism and combine the panel of selected features into radiomics signature and dosiomics signature for easy interpretation.[20] The performances of single dosiomics signature or radiomics signature seemed to be better than those of the dosimetric parameter, Sommat's model and Zhou's model in the training, validation, and prospective cohorts. The C-index increased when combining radiomics signature and dosiomics signature, which indicated that planning CT and dose distribution could complement each other in predicting radiation-induced injury. Not unexpectedly, the multiview radiomics risk model integrating radiomics signature, dosiomics signature, DVH parameter, and clinical factors had better results than Sommat's model and Zhou's model in terms of performance and generalization ability. In fact, the promising results of multiparametric model that combined radiomics, dosiomics, and clinical factors for predicting local control in skull-base chordoma have been reported.[15] The main reason may be that radiomics and dosiomics could make full use of the spatial information of planning CT and dose distribution, which carry microscopic genetic susceptibility of the thyroid and heterogeneity of the dose distribution. However powerful, underlying mechanism of radiomics and dosiomics features is still not fully explained, as the radiomics is inherently data-driven.[21,22] Following emerging approaches, the underlying biological mechanism of radiomics and dosiomics will be explored in the future. By using a multiview radiomics risk model, it was possible to precisely identify high-risk patients who required more regular monitoring of thyroid function after radiotherapy in clinical practice. In addition, when patients met the recommended dose constraint by Sommat's model or were in the low-risk group by Zhou's model, multiview radiomics risk model could still stratify patients into high-risk and low-risk groups, further demonstrating that it was superior to the other two models. Finally, the predicted hypothyroidism probabilities of two simulated treatment plans with same DVH parameter but different dose distributions by the multiview radiomics risk model were significantly different, while the two simulated plans had comparable predicted rates by Sommat's model or Zhou's model, which further verified the clinical application and advantage of the multiview radiomics risk model.

There were several advantages in this study. A multiview radiomics risk model was developed and validated to predict radiation-induced complications for the first time, combining radiomics, dosiomics, DVH parameters, and clinical factors. The multiview model provided a new

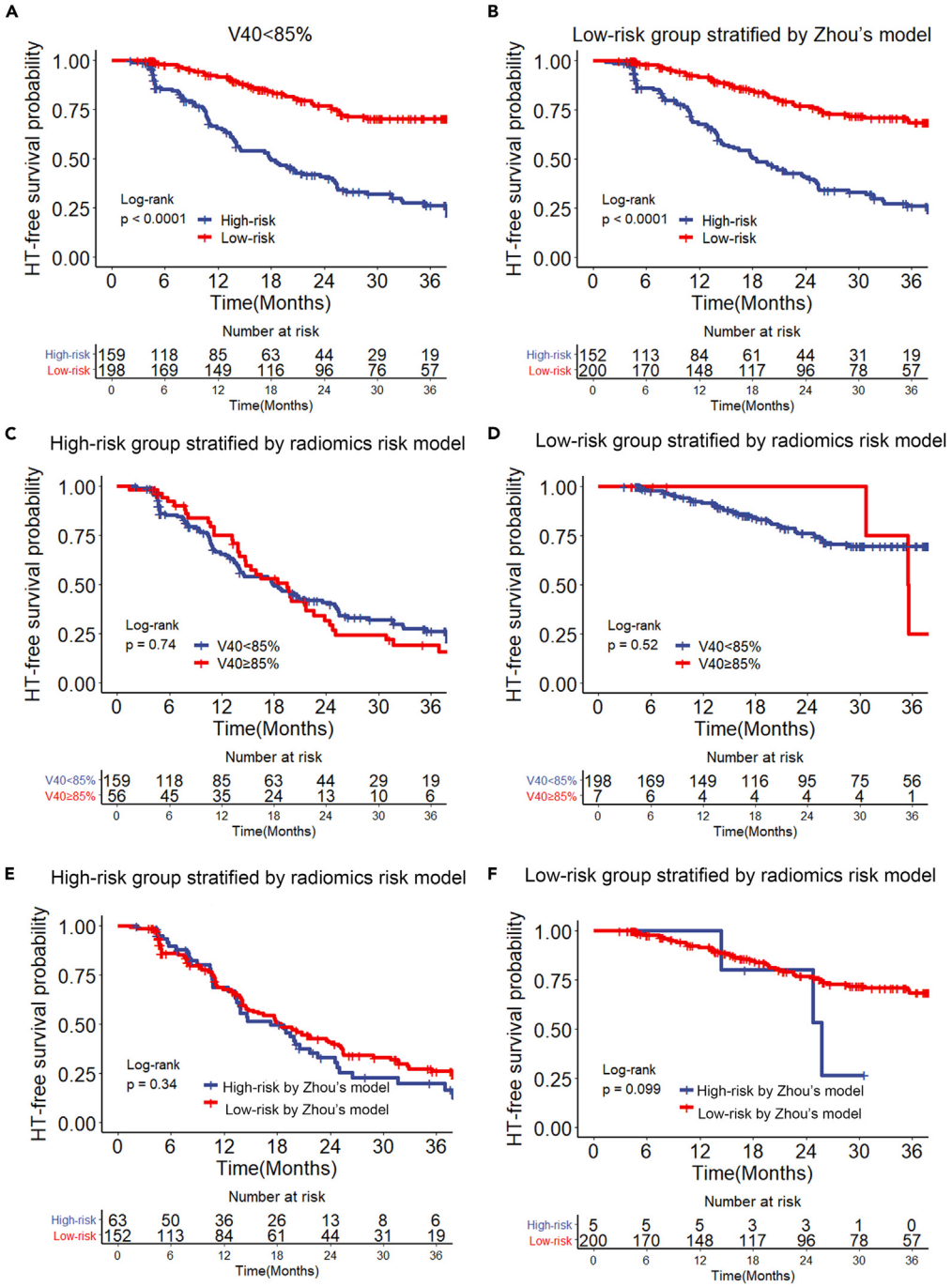

Figure 3. Hypothyroidism-free survival curves of subgroups

Hypothyroidism-free survival curves of high- and low-risk groups stratified by multiview radiomics risk model (A and B), V_{40} (C and D), and Zhou's model (E and F). (C and E) High-risk and (D and F) low-risk group stratified by multiview radiomics risk model.

Abbreviation: HT, hypothyroidism.

strategy for predicting other adverse events. Besides, imaging and segmentation perturbations evaluate the robustness of the selected features, contributing to the overall strength of the multiview radiomics risk model.

In conclusion, we developed and prospectively validated a multiview radiomics risk model to predict radiation-induced complications and guide IMRT. And the multiview radiomics risk model has better performance and generalization ability than existing models.

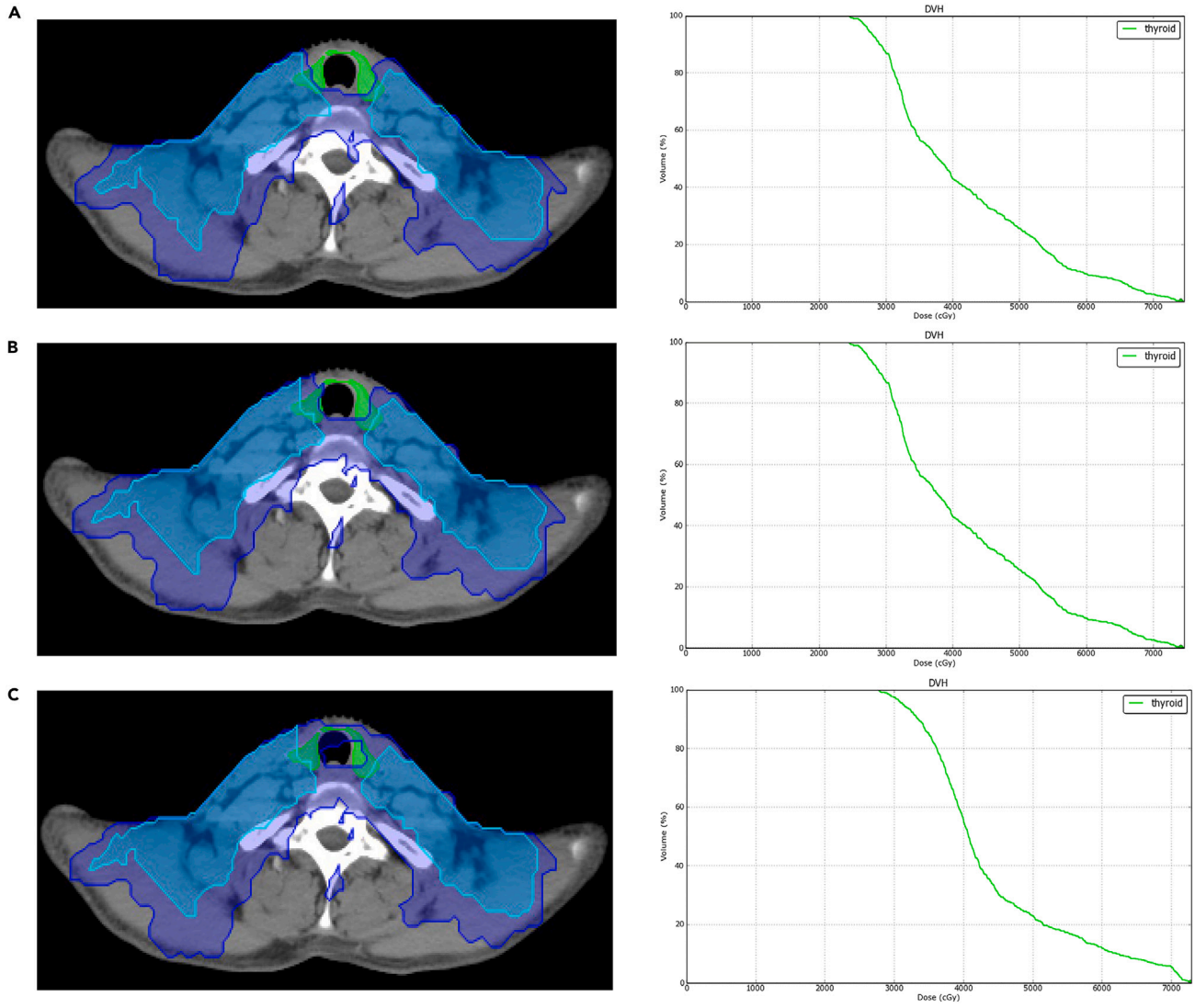

Figure 4. The 3D dose distributions and DVH curves of the redesigned simulated treatment plans
(A) Plan 1, (B) plan 2, (C) plan 3.
Abbreviation: DVH, dose-volume-histogram.

Limitations of the study

The limitations should also be noted. First, only radiation-induced hypothyroidism was evaluated in this study, and a more comprehensive model that could assess radiation-induced toxicities of multiple organs at risk and tumor volume is needed to guide future treatment plan design. Second, the multiview radiomics risk model was only validated in the prospective cohort, and external validation was needed in the future. Third, there was a lack of reporting the severity of hypothyroidism. In addition, although it is unclear how unfavorable texture features were improved during the optimization, dosiomics and radiomics were an important step in the right direction for automated planning using spatial dose volumes. A deep learning based multiview radiomics risk model with multicenter external tests is going to reduce time cost and improve performance.

STAR★METHODS

Detailed methods are provided in the online version of this paper and include the following:

- KEY RESOURCES TABLE
- RESOURCE AVAILABILITY

SUPPLEMENTAL INFORMATION

Supplemental information can be found online at https://doi.org/10.1016/j.isci.2023.108394.

ACKNOWLEDGMENTS

This work was funded by the Sun Yat-sen University Clinical Research 5010 Program (2015020), Guangdong Basic and Applied Basic Research Foundation (2022A1515110356), Medical Scientific Research Foundation of Guangdong Province (A2022367), and Guangzhou Science and Technology Program (2023A04J1788), Natural Science Foundation of Shandong Province (ZR202211260252).

AUTHOR CONTRIBUTIONS

Study design: P.Y.O.Y., S.S.Y., and F.Y.X. Data collection: P.Y.O.Y., B.Y.Z., S.S.Y., Z.Q.L., E.N.C., and A.Q.W. Data analysis: S.S.Y., A.Q.W., and Q.H.P. Writing original draft: P.Y.O.Y. and S.S.Y. Literature search: S.S.Y., C.Y.C., and Q.H.P. Resources: P.Y.O.Y., C.Y.C., and F.Y.X. Funding acquisition: F.Y.X., P.Y.O.Y., and C.Y.C. Supervision: F.Y.X. Review & editing: All authors.

DECLARATION OF INTERESTS

The authors declare no competing interests.

INCLUSION AND DIVERSITY

We support inclusive, diverse, and equitable conduct of research.

Received: April 3, 2023
Revised: June 28, 2023
Accepted: November 1, 2023
Published: November 4, 2023

REFERENCES

1. Chen, Y.-P., Chan, A.T.C., Le, Q.-T., Blanchard, P., Sun, Y., and Ma, J. (2019). Nasopharyngeal carcinoma. Lancet *394*, 64–80. https://doi.org/10.1016/s0140-6736(19)30956-0.
2. De Ruysscher, D., Niedermann, G., Burnet, N.G., Siva, S., Lee, A.W.M., and Hegi-Johnson, F. (2019). Radiotherapy toxicity. Nat. Rev. Dis. Prim. *5*, 13. https://doi.org/10.1038/s41572-019-0064-5.
3. Murthy, V., Narang, K., Ghosh-Laskar, S., Gupta, T., Budrukkar, A., and Agrawal, J.P. (2014). Hypothyroidism after 3-dimensional conformal radiotherapy and intensity-modulated radiotherapy for head and neck cancers: prospective data from 2 randomized controlled trials. Head Neck *36*, 1573–1580. https://doi.org/10.1002/hed.23482.
4. Lee, V., Chan, S.Y., Choi, C.W., Kwong, D., Lam, K.O., Tong, C.C., Sze, C.K., Ng, S., Leung, T.W., and Lee, A. (2016). Dosimetric Predictors of Hypothyroidism After Radical Intensity-modulated Radiation Therapy for Non-metastatic Nasopharyngeal Carcinoma. Clin. Oncol. *28*, e52–e60. https://doi.org/10.1016/j.clon.2016.05.004.
5. McDowell, L.J., Rock, K., Xu, W., Chan, B., Waldron, J., Lu, L., Ezzat, S., Pothier, D., Bernstein, L.J., So, N., et al. (2018). Long-Term Late Toxicity, Quality of Life, and Emotional Distress in Patients With Nasopharyngeal Carcinoma Treated With Intensity Modulated Radiation Therapy. Int. J. Radiat. Oncol. Biol. Phys. *102*, 340–352. https://doi.org/10.1016/j.ijrobp.2018.05.060.
6. Lertbutsayanukul, C., Kitpanit, S., Prayongrat, A., Kannarunimit, D., Netsawang, B., and Chakkabat, C. (2018). Validation of previously reported predictors for radiation-induced hypothyroidism in nasopharyngeal cancer patients treated with intensity-modulated radiation therapy, a post hoc analysis from a Phase III randomized trial. J. Radiat. Res. *59*, 446–455. https://doi.org/10.1093/jrr/rry036.
7. Zhou, L., Chen, J., Shen, W., Chen, Z.L., Huang, S., Tao, C.J., Chen, M., Yu, Z.H., and Chen, Y.Y. (2020). Thyroid V50 is a risk factor for hypothyroidism in patients with nasopharyngeal carcinoma treated with intensity-modulated radiation therapy: a retrospective study. Radiat. Oncol. *15*, 68. https://doi.org/10.1186/s13014-020-01490-x.
8. Sommat, K., Ong, W.S., Hussain, A., Soong, Y.L., Tan, T., Wee, J., and Fong, K.W. (2017). Thyroid V40 Predicts Primary Hypothyroidism After Intensity Modulated Radiation Therapy

for Nasopharyngeal Carcinoma. Int. J. Radiat. Oncol. Biol. Phys. *98*, 574–580. https://doi.org/10.1016/j.ijrobp.2017.03.007.

9. Zhai, R.P., Kong, F.F., Du, C.R., Hu, C.S., and Ying, H.M. (2017). Radiation-induced hypothyroidism after IMRT for nasopharyngeal carcinoma: Clinical and dosimetric predictors in a prospective cohort study. Oral Oncol. *68*, 44–49. https://doi.org/10.1016/j.oraloncology.2017.03.005.
10. Luo, R., Wu, V.W.C., He, B., Gao, X., Xu, Z., Wang, D., Yang, Z., Li, M., and Lin, Z. (2018). Development of a normal tissue complication probability (NTCP) model for radiation-induced hypothyroidism in nasopharyngeal carcinoma patients. BMC Cancer *18*, 575. https://doi.org/10.1186/s12885-018-4348-z.
11. Gillies, R.J., Kinahan, P.E., and Hricak, H. (2016). Radiomics: Images Are More than Pictures, They Are Data. Radiology *278*, 563–577. https://doi.org/10.1148/radiol.2015151169.
12. Huang, Y.Q., Liang, C.H., He, L., Tian, J., Liang, C.S., Chen, X., Ma, Z.L., and Liu, Z.Y. (2016). Development and Validation of a Radiomics Nomogram for Preoperative Prediction of Lymph Node Metastasis in Colorectal Cancer. J. Clin. Oncol. *34*, 2157–2164. https://doi.org/10.1200/JCO.2015.65.9128.
13. Rossi, L., Bijman, R., Schillemans, W., Aluwini, S., Cavedon, C., Witte, M., Incrocci, L., and Heijmen, B. (2018). Texture analysis of 3D dose distributions for predictive modelling of toxicity rates in radiotherapy. Radiother. Oncol. *129*, 548–553. https://doi.org/10.1016/j.radonc.2018.07.027.
14. Liang, B., Yan, H., Tian, Y., Chen, X., Yan, L., Zhang, T., Zhou, Z., Wang, L., and Dai, J. (2019). Dosiomics: Extracting 3D Spatial Features From Dose Distribution to Predict Incidence of Radiation Pneumonitis. Front. Oncol. *9*, 269. https://doi.org/10.3389/fonc.2019.00269.
15. Buizza, G., Paganelli, C., D'Ippolito, E., Fontana, G., Molinelli, S., Preda, L., Riva, G., Iannalfi, A., Valvo, F., Orlandi, E., and Baroni, G. (2021). Radiomics and Dosiomics for Predicting Local Control after Carbon-Ion Radiotherapy in Skull-Base Chordoma. Cancers *13*, 339. https://doi.org/10.3390/cancers13020339.
16. Lee, S.H., Han, P., Hales, R.K., Voong, K.R., Noro, K., Sugiyama, S., Haller, J.W., McNutt, T.R., and Lee, J. (2020). Multi-view radiomics and dosiomics analysis with machine learning for predicting acute-phase weight loss in lung cancer patients treated with radiotherapy. Phys. Med. Biol. *65*, 195015. https://doi.org/10.1088/1361-6560/ab8531.
17. Zhu, M.Y., Wu, H.J., Miao, J.J., Di, M.P., Chen, B.Y., Huang, H.G., Mai, H.Q., Wang, L., and Zhao, C. (2021). Radiation-induced hypothyroidism in patients with nasopharyngeal carcinoma treated with intensity-modulated radiation therapy with or without chemotherapy: Development of a nomogram based on the equivalent dose. Oral Oncol. *120*, 105378. https://doi.org/10.1016/j.oraloncology.2021.105378.
18. Wu, Y.H., Wang, H.M., Chen, H.H.W., Lin, C.Y., Chen, E.Y.C., Fan, K.H., Huang, S.F., Chen, I.H., Liao, C.T., Cheng, A.J., and Chang, J.T.C. (2010). Hypothyroidism after radiotherapy for nasopharyngeal cancer patients. Int. J. Radiat. Oncol. Biol. Phys. *76*, 1133–1139. https://doi.org/10.1016/j.ijrobp.2009.03.011.
19. Peng, L., Mao, Y.P., Huang, C.L., Guo, R., Ma, J., Wen, W.P., and Tang, L.L. (2020). A New Model for Predicting Hypothyroidism After Intensity-Modulated Radiotherapy for Nasopharyngeal Carcinoma. Front. Oncol. *10*, 551255. https://doi.org/10.3389/fonc.2020.551255.
20. Peng, H., Dong, D., Fang, M.J., Li, L., Tang, L.L., Chen, L., Li, W.F., Mao, Y.P., Fan, W., Liu, L.Z., et al. (2019). Prognostic Value of Deep Learning PET/CT-Based Radiomics: Potential Role for Future Individual Induction Chemotherapy in Advanced Nasopharyngeal Carcinoma. Clin. Cancer Res. *25*, 4271–4279. https://doi.org/10.1158/1078-0432.CCR-18-3065.
21. Tomaszewski, M.R., and Gillies, R.J. (2021). The Biological Meaning of Radiomic Features. Radiology *298*, 505–516. https://doi.org/10.1148/radiol.2021202553.
22. Yang, S.S., OuYang, P.Y., Guo, J.G., Cai, J.J., Zhang, J., Peng, Q.H., He, Y., Zhang, B.Y., Liu, Z.Q., Hu, X.F., et al. (2023). Dosiomics Risk Model for Predicting Radiation Induced Temporal Lobe Injury and Guiding Individual Intensity-Modulated Radiation Therapy. Int. J. Radiat. Oncol. Biol. Phys. *115*, 1291–1300. https://doi.org/10.1016/j.ijrobp.2022.11.036.
23. Collins, G.S., Reitsma, J.B., Altman, D.G., and Moons, K.G.M. (2015). Transparent reporting of a multivariable prediction model for individual prognosis or diagnosis (TRIPOD): the TRIPOD Statement. BMC Med. *13*, 1. https://doi.org/10.1186/s12916-014-0241-z.
24. Sun, Y., Yu, X.L., Luo, W., Lee, A.W.M., Wee, J.T.S., Lee, N., Zhou, G.Q., Tang, L.L., Tao, C.J., Guo, R., et al. (2014). Recommendation for a contouring method and atlas of organs at risk in nasopharyngeal carcinoma patients receiving intensity-modulated radiotherapy. Radiother. Oncol. *110*, 390–397. https://doi.org/10.1016/j.radonc.2013.10.035.

STAR★METHODS

KEY RESOURCES TABLE

REAGENT or RESOURCE	SOURCE	IDENTIFIER
Deposited data		
clinical data of patients	Research Data Deposit Management Committee	https://www.researchdata.org.cn/
planning computed tomography	Sun Yat-sen University cancer center	N/A
dose distribution	Sun Yat-sen University cancer center	N/A
Software and algorithms		
R 4.1.0	R Development Core Team	https://cran.r-project.org/
Python 3.0.1	Python Development Core Team	https://www.python.org/

RESOURCE AVAILABILITY

Lead contact

Further information and requests for resources and reagents should be directed to and will be fulfilled by the lead contact, Chun-Yan Chen (chenchuny@sysucc.org.cn).

Materials availability

This study did not generate new unique reagents.

Data and code availability

The radiological images, radiotherapy plans and clinical data are available from the lead contact upon reasonable request. This paper does not report original code. Any additional information required to reanalyze the data reported in this paper is available from the lead contact upon request.

EXPERIMENTAL MODEL AND STUDY PARTICIPANT DETAILS

Ethics statement

This study was approved by the Ethics Committees of our Center (B2021-343), and informed consent was obtained from all eligible patients.

Patients

A total of 803 nasopharyngeal carcinoma patients who received intensity-modulated radiotherapy between January 2014 and December 2015 at Sun Yat-sen University Cancer Center were retrospectively enrolled for the training cohort (n = 723) and validation cohort (n = 80). The inclusion criteria were as follows (1) age greater than 18 years, regardless of gender and ethnicity, newly diagnosed, untreated nasopharyngeal carcinoma; (2) receipt of one course of intensity-modulated radiotherapy; (3) normal thyroid function before radiotherapy; (4) the availability of the radiotherapy treatment plan; and (5) regular follow-up of thyroid function. Exclusion were patients (1) who underwent thyroidectomy; (2) who received irradiation to pituitary and/or head and neck cancer; (3) with disorders in the hypothalamic-pituitary-thyroid axis before radiotherapy; (4) with thyroid tumors; and (5) who were diagnosed with central hypothyroidism. All patients were restaged according to 8th edition American Joint Committee on Cancer/Union for International Cancer Control (AJCC/UICC) staging system.

In addition, 420 patients from the secondary analysis of our prospective observational study (ClinicalTrials.gov Identifier: NCT03003182) since May 2017 were defined as the prospective test cohort. This study was approved by the Ethics Committees of our Center (B2021-343), and informed consent was obtained from all eligible patients. The study followed the transparent reporting of a multivariable prediction model for individual prognosis or diagnosis (TRIPOD) guidelines.[23]

METHOD DETAILS

Evaluation of hypothyroidism

Thyroid function was evaluated before radiotherapy, including serum levels of thyroid-stimulating hormone (TSH), free triiodothyronine (FT3), and free thyroxine (FT4). After radiotherapy, all eligible patients were followed-up for thyroid function every three months during the first two years, and then every six months. Thyroid function was measured using the electrochemiluminescence method (Elecsys 2010 analyzer) in our center. The reference ranges of TSH, FT3, and FT4 were 0.27–4.20 μIU/mL, 2.80–7.10 pmol/L, and 12.00–22.00 pmol/L, respectively. Primary hypothyroidism was defined as elevated TSH (>4.20 μIU/mL) with normal or low FT4 levels (<22.00 pmol/L).

Treatment and follow up

All participants were treated with radical intensity-modulated radiotherapy. The delineation of target volumes was consistent with the International Commission on Radiation Units and Measurements Reports 50 and 62. The prescribed doses were 66–72 Gy/28–33 fractions to gross tumor and 64–70 Gy/28–33 fractions to lymph node, 60–63 Gy/28–33 fractions to the high-risk clinical target volume (CTV1), and 54–56 Gy/28–33 fractions to the low-risk clinical target volume (CTV2). The dose to organs at risk was restricted referring to the Radiation Therapy Oncology Group 02-25 protocol. The organs at risk were delineated according to recommendations by Sun et al.[24] Radiotherapy alone was the main treatment modality for stage I nasopharyngeal carcinoma, while concurrent chemotherapy with or without induction chemotherapy was recommended for stage II-IV disease based on the National Comprehensive Cancer Network (NCCN) guidelines.

After treatment, follow-up was performed every 3 to 6 months during the first 2 years and then every 6 to 12 months thereafter. The duration of follow-up was defined from the beginning of primary intensity-modulated radiotherapy to the onset of hypothyroidism or the final examination of thyroid function. The endpoint was hypothyroidism-free survival, which was calculated from the start of radiotherapy to the occurrence of hypothyroidism.

Planning CT and dose distribution protocol

All patients were immobilized in the supine position using a head-neck-shoulder thermoplastic mask. Planning CT images, which acquired from CT simulation positioning system (Philips, Brilliance Big Bore), were ranged from the head to 2 cm below the sternoclavicular joint with 3 mm slices, a matrix size of 512 × 512, and voxel resolution of 0.97 × 0.97 × 3.0 mm in the left-right, anteroposterior, and craniocaudal directions. The CT scanning parameters were as follows: voltage of 140 kV, scanning current of 280 mAs, scanning slice thickness of 3 mm, and reconstruction layer thickness of 3 mm. The image reconstruction algorithm was iterative reconstruction algorithm, while the dose calculation algorithm was Algorithm Architecture Adequation (AAA). And the CT value-to-tissue density conversion curve was employed for tissue inhomogeneity correction and absorbed dose distribution calculation.

Image segmentation and dosimetric parameters

Radiotherapy planning CT and dose distribution were obtained from the treatment planning system (Version 15.6, Eclipse, Varian, CA, USA). All thyroids, as regions of interest, were re-delineated using ITK-SANP software (version 3.8.0; www.itksnap.org) on planning CT images by a radiation oncologist (PYOY) with ten years of experience, and checked again by an expert radiation oncologist (FYX) with over 30 years of experience.[24] Dosimetric parameters were extracted from the treatment plan, including V_5-V_{70} in V_5 increments (V_x, the percentage of thyroid receiving over X Gy), thyroid volume, the mean, maximum, minimum dose (D_{mean}, D_{max}, D_{min}), $D_{0.5cc}$, and D_{1cc} (dose to 0.5 ml or 1 ml of thyroid). All dosimetric parameters were rescaled to an equivalent dose of 2 Gy per fraction (EQD_{2Gy}) by a linear quadratic model. The process was performed by using MATLAB (MathWorks, Natick, MA).

To allow for direct comparison with previous studies, a linear quadratic model was used to rescale DVH to an equivalent dose of 2 Gy per fraction (EQD_2Gy).

$$EQD2Gy = Dx * (\alpha/\beta + dx)/(\alpha/\beta + 2)$$

$$\mathrm{Dx} = \text{total dose}, \mathrm{dx} = \text{dose per fraction}, \text{and } \alpha/\beta = 3 \text{ Gy}$$

Feature extraction

Radiotherapy simulated CT and dose distribution were obtained from the treatment planning system (Version 15.6, Eclipse, Varian, CA, USA). Radiomics features and dosiomics features were extracted from simulated CT and 3D dose distributions using the "pyradiomics" package in Python (version 3.0.1). A filtering process was conducted to make the image smooth and reveal the detailed information of the original image from different directions and levels. The filtered images were generated by performing a low-/high-pass "Coiflet 1" wavelet filter on the original image in the x-/y-/z-direction separately. Assume that L, H and X represent the low-pass function, high-pass function, and original images respectively. Thus, eight filtered images were labeled as X_{LLL}, X_{LLH}, X_{LHL}, X_{LHH}, X_{HLL}, X_{HLH}, X_{HHL}, and X_{HHH}. In addition, the Laplacian of Gaussian (LoG) filter was also applied to the original image, and the corresponding image was derived for each sigma. Since the sigma value was specified as 1 mm to 5 mm in this study, five derived images were obtained. Finally, 1316 quantitative radiomics features and 1302 dosiomics features were extracted, including 14 shape features from original images, 14*18 first order features, and 14*75 texture features (24 Gray Level Co-occurrence Matrix, GLCM; 16 Gray Level Run Length Matrix, GLRLM; 16 Gray Level Size Zone Matrix, GLSZM; 14 Gray Level Dependence Matrix, GLDM; 5 Neighboring Gray Tone Difference Matrix, NGTDM) from original images and corresponding filtered images. Feature extraction was standardized according to the Image Biomarker Standardization Initiative (IBSI). For more information about formulas for computing these features, please visit https://pyradiomics.readthedocs.io/en/latest/.

All extracted features were standardized by z-score method.

Z-score:

$$z = (x - \mu)/\sigma$$

x is the original feature value, z is the normalized feature value, $\boldsymbol{\mu}$ is the mean of the feature value, and $\boldsymbol{\sigma}$ is the standard deviation of the feature value.

Feature selection and signature building

For each thyroid, 1316 radiomics features and 1302 dosiomics features were extracted from planning CT and dose distribution using Python software, including shape, first order, and five kinds of texture features (Gray Level Co-occurrence Matrix (GLCM), Gray Level Size Zone Matrix (GLSZM), Gray Level Dependence Matrix (GLDM), Gray Level Run Length Matrix (GLRLM), and Neighbouring Gray Tone Difference Matrix (NGTDM)). First-order statistics describe the distribution of voxel intensities in the ROI without considering spatial relationships. Texture features of image, including GLCM, GLDM, GLSZM, NGTDM, describe statistical interrelationships between voxels with contrast values. And wavelets filter and Laplacian of Gaussian (LoG) filter were conducted to reveal the detailed information of the original image from different directions and levels. For more information, please visit https://pyradiomics.readthedocs.io/en/latest/. And radiomics features and dosiomics features, which were standardized using z-score, were then selected for signature building. Feature selection and signature building were conducted to remove irrelevant and redundant features. Both feature selection and model building were conducted in the training cohort. First, univariate Cox proportional hazard regression model was applied to select features that were potential predictors for hypothyroidism-free survival. Only features with $p < 0.05$ were chosen for the next step. Second, Pearson correlation analysis was conducted to remove the redundant features using the "find Correlation" function of the "caret" package in R software. The Pearson correlation coefficients (r) of pairwise features and the mean absolute correlation of each feature were calculated. Highly correlated features were selected from a correlation matrix. If the Pearson |r| of pairwise feature is greater than 0.8, the feature with the largest mean absolute correlation was removed. Next, the least absolute shrinkage and selection operator (LASSO) Cox regression method was conducted to identify useful predictors for hypothyroidism-free survival. The tuning parameter (λ) in the LASSO model was determined using 10-fold cross-validation with minimum criteria (Table S2). Finally, selected dosiomics features and radiomics features were combined into a dosiomics signature and a radiomics signature based on a linear combination of selected features, which weighed by their coefficients, respectively (Table S3).

$$\begin{aligned}\textit{Dosiomics score} = {} & -0.026*\textit{wavelet.HHH\_firstorder\_Kurtosis} - 0.146*\textit{wavelet.LLL\_glcm\_ClusterProminence} \\ & - 0.030*\textit{log.sigma.3.0.mm.3D\_glcm\_Idn} + 0.005*\textit{wavelet.LHL\_glcm\_MaximumProbability} \\ & - 0.009*\textit{wavelet.LLL\_glcm\_MCC} - 0.003*\textit{wavelet.LHH\_glcm\_MaximumProbability} \\ & - 0.074*\textit{wavelet.HLH\_gldm\_DependenceNonUniformityNormalized} \\ & - 0.046*\textit{wavelet.LHH\_gldm\_DependenceNonUniformityNormalized} \\ & - 0.046*\textit{wavelet.HHL\_gldm\_LargeDependenceLowGrayLevelEmphasis} \\ & - 0.044*\textit{original\_gldm\_DependenceNonUniformity} - 0.031*\textit{wavelet.HHL\_gldm\_} \\ & \quad \textit{DependenceNonUniformityNormalized} - 0.024*\textit{wavelet.LLL\_gldm\_} \\ & \quad \textit{LargeDependenceHighGrayLevelEmphasis} - 0.017*\textit{wavelet.HLH\_} \\ & \quad \textit{gldm\_LargeDependenceHighGrayLevelEmphasis} - 0.024*\textit{wavelet.LHL\_glrlm\_} \\ & \quad \textit{RunLengthNonUniformity} - 0.052*\textit{log.sigma.5.0.mm.3D\_glszm\_SmallAreaHighGrayLevelEmphasis} \\ & - 0.044*\textit{wavelet.HHH\_glszm\_SmallAreaHighGrayLevelEmphasis} - 0.002*\textit{wavelet.HHH\_glszm\_} \\ & \quad \textit{SmallAreaLowGrayLevelEmphasis} + 0.005*\textit{wavelet.LHH\_glszm\_SizeZoneNonUniformityNormalized} \\ & + 0.008*\textit{original\_glszm\_SmallAreaLowGrayLevelEmphasis} + 0.018*\textit{wavelet.LHL\_glszm\_ZonePercentage}\end{aligned}$$

$$\begin{aligned}\textit{Radiomics score} = {} & -0.005*\textit{original\_shape\_LeastAxisLength} - 0.052*\textit{wavelet.LHH\_firstorder\_Median} - 0.042*\textit{wavelet.HLH\_} \\ & \quad \textit{firstorder\_Maximum} - 0.018*\textit{wavelet.HLL\_firstorder\_10Percentile} - 0.008*\textit{wavelet.HHL\_firstorder\_} \\ & \quad \textit{Skewness} + 0.035*\textit{wavelet.LLH\_firstorder\_Skewness} + 0.065*\textit{original\_firstorder\_} \\ & \quad \textit{RobustMeanAbsoluteDeviation} + 0.082*\textit{wavelet.LHL\_firstorder\_90Percentile} + 0.029*\textit{wavelet.LHL\_} \\ & \quad \textit{firstorder\_InterquartileRange} - 0.058*\textit{original\_glcm\_MCC} - 0.064*\textit{wavelet.HHH\_glcm\_} \\ & \quad \textit{SumAverage} - 0.057*\textit{log.sigma.3.0.mm.3D\_gldm\_DependenceEntropy} - 0.020*\textit{wavelet.LHL\_gldm\_} \\ & \quad \textit{SmallDependenceLowGrayLevelEmphasis} - 0.010*\textit{wavelet.LHL\_gldm\_} \\ & \quad \textit{DependenceVariance} + 0.003*\textit{wavelet.HHL\_gldm\_SmallDependenceHighGrayLevelEmphasis} \\ & + 0.008*\textit{wavelet.HHH\_gldm\_LowGrayLevelEmphasis} + 0.029*\textit{wavelet.HLH\_gldm\_DependenceEntropy} \\ & + 0.041*\textit{wavelet.LLH\_gldm\_DependenceEntropy} + 0.054*\textit{log.sigma.5.0.mm.3D\_gldm\_} \\ & \quad \textit{SmallDependenceHighGrayLevelEmphasis} - 0.062*\textit{wavelet.HLL\_glszm\_SizeZoneNonUniformity} \\ & - 0.050*\textit{wavelet.HHH\_glszm\_SizeZoneNonUniformity} - 0.045*\textit{wavelet.LHL\_glszm\_} \\ & \quad \textit{LargeAreaLowGrayLevelEmphasis} - 0.027*\textit{wavelet.HLH\_glszm\_LargeAreaHighGrayLevelEmphasis} \\ & - 0.004*\textit{wavelet.LHH\_glszm\_SizeZoneNonUniformity} + 0.001*\textit{wavelet.HHL\_glszm\_} \\ & \quad \textit{LowGrayLevelZoneEmphasis} + 0.128*\textit{log.sigma.2.0.mm.3D\_glszm\_SmallAreaLowGrayLevelEmphasis} \\ & - 0.007*\textit{log.sigma.5.0.mm.3D\_ngtdm\_Busyness}\end{aligned}$$

Robustness evaluation of the selected features

Imaging and Segmentation (for thyroid) perturbations are performed for robustness evaluation of the selected features. The features extracted from the derived CTs and dose distributions were assessed by the intraclass correlation coefficient (ICC), and features with an ICC higher than 0.8 were considered robustness.

Imaging perturbations were performed by modifying the reconstruction parameters of the planning CT, thus generating several sets of derived CTs on the large-aperture CT simulation localizer (GE Discovery CT590RT). 1) Modify the field of view (FOV): set FOV to 50 and 60 respectively, while the rest of the reconstruction parameters are the same, thereby reconstructing two sets of derived CTs; 2) Modify the reconstruction mode: set it to "Soft", "Stnd" and "Detail" respectively, and the rest of the reconstruction parameters are the same, generating three sets of derived CTs. Segmentation perturbations were conducted by test-retest and inter-rater analyses. For test-retest analysis, a radiation oncologist (PYOY) delineated the thyroids on 38 randomly selected patients twice, with a 6-month interval between outlines. And two radiation oncologists (PYOY and SSY) delineated the thyroids respectively, to perform the inter-rater analyses. To evaluate the robustness of dosiomics features, we modified the dose calculation grid size to 0.2cm, 0.25cm, and 0.3cm, respectively. We recalculate the dose and generate three sets of derived dose distributions.

QUANTIFICATION AND STATISTICAL ANALYSIS

The endpoint was primary hypothyroidism-free survival, which was calculated from the beginning of intensity-modulated radiotherapy to the occurrence of primary hypothyroidism.

The chi-square test was used to compare the clinical variables. Potential clinical factors for predicting hypothyroidism were selected by univariate Cox regression (Table S1). Since dosimetric parameters are highly correlated with each other, the most critical factor was select according to the maximum area under the receiver operating curve (AUC). The potential multiview data, which consisted of clinical risk factors, dosimetric parameter, dosiomics signature, and radiomics signature were incorporated into multivariable Cox regression to build a multiview model for predicting hypothyroidism. The stepwise regression model was performed with Akaike's information criterion, and multicollinearity of variables in the model was evaluated by the variance inflation factor (VIF). The variables with a VIF higher than 5 were removed.

To improve the stability and reproducibility of the model, the training and validation cohorts were randomly assigned using 10-fold cross-validation. Harrell's concordance index (C-index) and the AUC of receiver operating characteristic (ROC) curve were used to evaluate the performance of the model and compare it with Sommat's model of V_{40}[8] and Zhou's model of thyroid volume plus N stage.[7] Calibration curve was plotted to access the agreement between the predicted probability of multiview radiomics risk model and the actual outcome. Decision curve analysis was used to evaluate the net benefits of the model at specific threshold probabilities. The cutoff value of different risk groups was determined by time-dependent ROC, and the survival curves were compared using Kaplan–Meier with log-rank test.

To further verify the clinical application of the multiview radiomics risk model, 50 test patients (29 hypothyroidism and 21 euthyroid patients) were randomly selected. Three different simulated treatment plans were redesigned for each patient, including a simulated plan that was very similar to the irradiated treatment plan and two different simulated plans with the same DVH parameters but different dose distributions. The predicted hypothyroidism-free probability of different simulated plans was compared by the Wilcoxon matched-pairs signed rank test.

Statistical analysis was conducted in R software (https://cran.r-project.org/). The p values of the C-index were computed by the "Hmisc" package in R software. A p value < 0.05 (two-sided) was considered statistically significant. The C-index values of 0.5–0.7, 0.7–0.9, and 0.9–1 indicated low, medium, and high predictive accuracy, respectively.